HHS Public Access

Author manuscript

Mitochondrion. Author manuscript; available in PMC 2022 June 16.

Published in final edited form as:

Mitochondrion. 2021 September ; 60: 129–141. doi:10.1016/j.mito.2021.08.005.

ATPAF1 deficiency impairs ATP synthase assembly and mitochondrial respiration

Zhou Zhou[a],

Kailiang Zhang[a],

Zhiheng Liu[a],

Xu Gao[a],

Kai Huang[b],

Chen Chen[a],

Daowen Wang[a],

Qinglin Yang[c,e,*],

Qinqiang Long[a,d,e,*]

[a]Division of Cardiology, Department of Internal Medicine, Tongji Hospital, Tongji Medical College, Huazhong University of Science and Technology, 1095 Jiefang Ave, Wuhan 430030, China

[b]Department of Cardiovascular Diseases, Union Hospital, Tongji Medical College, Huazhong University of Science and Technology, Wuhan 430022, China

[c]Cardiovascular Center of Excellence and Department of Pharmacology, Louisiana State University Health Science Center-New Orleans, LA 70112, United States

[d]Guangdong Metabolic Diseases Research Center of Integrated Chinese and Western Medicine, Institute of Chinese Medicine, Guangdong Pharmaceutical University, Guangzhou 510006, China

[e]Department of Nutrition Science, University of Alabama at Birmingham, Birmingham, AL 35294, United States

Abstract

ATP11p and ATP12p are two nuclear-encoded mitochondrial chaperone proteins required for assembling the F1Fo-ATP synthase F1 sector. ATPAF1 and ATPAF2 are the mammalian homologs of ATP11p and ATP12p. However, the biochemical and physiological relevance of ATPAF1 and ATPAF2 in animal tissues with high energy-dependence remains unclear. To explore the *in vivo* role of ATP assembly and the effects of ATP synthase deficiency in animals, we have generated

*Corresponding authors at: Cardiovascular Center of Excellence, Louisiana State University Health Science Center, 533 Bolivar St. 4th Fl, Rm 416, New Orleans, LA 70112, United States (Q. Yang). Guangdong Metabolic Diseases Research Center of Integrated Chinese and Western Medicine, Institute of Chinese Medicine, Guangdong Pharmaceutical University, 280 Wai Huan Dong Road, Guangzhou Higher Education Mega Center, Guangzhou 510006, China (Q. Long). qyang1@lsuhsc.edu (Q. Yang), longqq@aliyun.com, longqq@gdpu.edu.cn (Q. Long).

Declaration of Competing Interest

The authors declare that they have no known competing financial interests or personal relationships that could have appeared to influence the work reported in this paper.

Appendix A. Supplementary data

Supplementary data to this article can be found online at https://doi.org/10.1016/j.mito.2021.08.005.

knockout (KO) mouse models of these assembly factors using CRISPR/Cas9 technology. While the *Atpaf2*-KO mice were embryonically lethal, *Atpaf1*-KO mice grew to adulthood but with smaller body sizes and elevated blood lactate later in life. We specifically investigated how ATPAF1 deficiency may affect ATP synthase biogenesis and mitochondrial respiration in the mouse heart, an organ highly energy-dependent. Western blots and Blue-Native electrophoresis (BN-PAGE) demonstrated a decreased F1 content and ATP synthase dimers in the *Atpaf1*-KO heart. Mitochondria from ATPAF1-deficient hearts showed ultrastructural abnormalities with condensed degenerated mitochondria, loss of cristae, and impaired respiratory capacity. ATP synthase deficiency also leads to impaired autophagy and mitochondrial dynamic. Consequently, decreased cardiac function was exhibited in adult *Atpaf1*-KO mice. The results provide strong support that ATPAF1 is essential for ATP synthase assembly and mitochondrial oxidative phosphorylation, thus playing a crucial role in maintaining cardiac structure and function in animals.

Keywords

Mitochondrial dysfunction; Mitochondria; ATP synthase assembly; Oxidative phosphorylation (OXPHOS)

1. Introduction

Mitochondrial ATP synthase (or F1Fo-ATP synthase) is a crucial enzymatic complex and an ATP generator utilizing the proton motive force from mitochondrial electron transport chain. ATP synthase generates more than 90% of cellular ATP, the energy currency (Artika, 2019; Nakamoto et al., 2008), in eukaryotic cells under aerobic conditions (Kabaleeswaran et al., 2006; Srivastava et al., 2018). ATP synthase deficiencies are associated directly, or indirectly with various human diseases, such as Leigh syndrome (a neurodegenerative disease) (de Vries et al., 1993), neuropathy, ataxia, retinitis pigmentosa syndrome or syndromes characterized by severe lactic acidosis and cardiomyopathy (Ghezzi and Zeviani, 2018; Hong and Pedersen, 2008).

ATP synthase is comprised of the Fo sector in the inner membrane and the connected F1 sector in the matrix. ATP synthase operates by a rotary catalytic mechanism where proton translocation through the Fo region is coupled to ATP synthesis in the catalytic F1 region via rotation of a central rotor subcomplex (Zhou et al., 2015). The F1 catalytic domain is mainly composed of the $(\alpha\beta)_3$ subcomplex (Stock et al., 2000). Previous studies indicate that the incorporation of α and β subunits of yeast F1 depends on at least two assembly factors, ATP11 and ATP12 homologs (Ackerman and Tzagoloff, 1990) (Supplementary S1), which are nuclear-encoded proteins located in yeast mitochondria (Ackerman et al., 1992; Bowman et al., 1991). ATP11 knockout (KO) Yeast display ATPase (ATP hydrolysis) deficiency (Ackerman and Tzagoloff, 1990). ATPAF1 and ATPAF2 are mammalian homologues of ATP11 and ATP12 (Wang et al., 2001). In experiments conducted in yeast, fusion proteins containing human ATPAF1 or ATPAF2 and the DNA binding domain of galactose-responsive transcription factor (Gal4p) is respectively interacting with the β subunit and α subunit (Wang et al., 2001). However, the interactions between ATPAF1/2 with the F1

subunits have never been validated in mammalian cells and the F1 assembly effects of ATPAF1/2 remain unvalidated. Interestingly, a first human case of ATP synthase deficiencies due to an ATP12 (ATPAF2) mutation was identified with characteristics that resembled Cerebro-oculofacioskeletal (COFS) syndrome (De Meirleir et al., 2004). However, most of our current understanding of ATPAF1 and ATPAF2 is derived from studies based on yeast. The potential role of ATPAF1 and ATPAF2 in ATP synthase assembly and the subsequent pathophysiological consequences in mammals remain obscure. Studies in animals should uncover the role of these assembling factors in ATP synthase activity and how they affect mitochondrial homeostasis in the *in vivo* context.

In the present study, we investigate a mouse model with *Atpaf1* knockout to gain insights into the *in vivo* function of ATPAF1 in animals. Since ATP synthase generates most ATP in the highly energy-dependent heart, we focused on uncovering the effects of ATPAF1 deficiency on the biogenesis of ATP synthase and mitochondrial respiration in mouse heart. We found that ATPAF1 is essential to maintain mitochondrial fitness because of its essential role in ATP synthase assembly and function. The lack of ATPAF1 in mice leads to cardiac dysfunction. Results from the study yield novel insights into the role of ATPAF1-mediated ATP synthase biogenesis and the pathophysiological implications of ATP synthase deficiency in the heart.

2. Materials and methods

2.1. Mice

All animals were housed in temperature-controlled cages under a 12-h light-dark cycle and given free access to water and normal chow. All animal experiments were conducted following the National Institute of Health Guide for the Care and Use of Laboratory Animals and were approved by the Committee on the Ethics of Animal Experiments of Tongji Medical College. The *Atpaf1* knockout (KO) mice were generated by Cyagen Biosciences using the CRISPR/Cas9 technique. Genotyping of the offspring was detected via PCR analysis and gel agarose electrophoresis. The sequences of the primers are listed in Supplementary Table 1. And wild type C57BL/6J mice (Beijing Vital River Laboratory Animal Technology Co., Ltd, Beijing, China) were used as the control group. This study was approved by the Animal Research Committee of Tongji Medical College, Huazhong Science and Technology University.

2.2. Cell culture, transfection and co-immunoprecipitation (Co-IP)

HEK293 cells were cultured in Dulbecco's Modified Eagle's Medium (DMEM) with 10% fetal bovine serum, 100 U/ml penicillin, and 100 μg/ml streptomycin. Cells were maintained at 37 °C under humidified conditions, 5% CO_2. HEK293 cells were transfected with *Atpaf1*-Flag plasmid using PolyJet™ (Signagen Laboratories, MD, US), according to the manufacturer's instructions. Briefly, cells were plated on 10-cm dishes to obtain ~80% confluency at the time of transfection (on the second day). Plasmid containing *Atpaf1* (5 μg/ml) were diluted in 500 μl of serum-free DMEM and vortexed briefly to mix. Then 15 μl of PolyJet™ reagent were added, vortexed to mix, and incubated for 10 min at room temperature. After that, transfection mix was added to the cells in 5 ml serum-containing

medium and gene expression 48 h post-transfection was measured. Transfected HEK293 cells were washed once in PBS then lysed in lysis buffer (20 mM Tris (pH7.5), 150 mM NaCl, 1% Triton X-100) on ice for 10–15 min. Unbroken cells and nuclei were removed by centrifugation at 12 000g for 10 min. Supernatant fractions were immunoprecipitated using Anti-Flag magnetic beads (Bimake, Texas, US), according to the manufacturer's instructions. For reciprocal IP, the antibody ATP5B was incubated first with Protein A/G magnetic beads (Bimake, Texas, US), followed by addition of the transfected HEK293 (pc*Atpaf1*-Flag plasmid) cells lysate at 4 °C overnight. Then the antigen eluted from the support was immunoprecipitated by SDS-PAGE.

2.3. Immunofluorescence staining

AC16 cells were transfected with pc*Atpaf1*-Flag plasmid using PolyJet™ (Signagen Laboratories, MD, US), according to the manufacturer's instructions. Subcellular localization was measured 48 h post-transfection. Transfected AC16 cells were washed twice in phosphate buffer saline (PBS) and fixed using 4% formaldehyde fixative at room temperature for 15 min. Then the cells were permeabilized by incubating in 1% Triton X-100 at room temperature for 15 min. Next, cells were blocked with 5% goat serum in PBS at room temperature for 1 h, then incubated with primary antibodies against ATP5B (1:200, ABclonal Biotechnology, Wuhan, China) and anti-Flag (1:500, Proteintech Group, Inc, USA) at 4 °C overnight, followed by incubation with secondary anti-rabbit and anti-mouse fluorescent antibodies (1:500, Boster Biological Tech, Wuhan, China) at room temperature for 1 h. Then we observed and analyzed the images by fluorescence microscope.

2.4. Echocardiography

Transthoracic echocardiography was used to assess cardiac function and anatomical changes in mice using a Vevo 1100 Imaging System (Visual Sonics, Toronto, Canada) equipped with a 30 MHz linear-array transducer. M-mode tracings in parasternal short-axis view were used to measure left ventricular (LV) and posterior wall thickness and left ventricular internal diameter at end-systole and end-diastole, which were used to calculate left ventricular fractional shortening and ejection fraction.

2.5. RNA isolation, quantitative real-time PCR and semi-quantitative RT-PCR

Total RNA from dissected ventricular heart tissue samples was isolated with TRIzol reagent (Invitrogen). Total RNA (500 ng) was reverse-transcribed into cDNA using hexametric random primers followed by qPCR for genes related to hypertrophy (Anp/Nppa: natriuretic peptide type A), heart failure (Bnp/Nppb: natriuretic peptide type B) and the superoxide related gene (Nox4; Sod1; Sod2; Gpx1) according to the manufacturer's instructions. The housekeeping gene Actin and Gapdh were used for normalization. Gene expression was calculated with the $2^{-\Delta\Delta Ct}$ method. For semi-quantitative RT-PCR, the cycle number was optimized for the primers including the housekeeping gene by analyzing gel intensity from 15 to 30 cycles to make sure that PCR was conducted in linear range of amplification. Gapdh was used as a reference gene. PCR products were resolved in 1% agarose gels. The sequences of the primers are listed in Supplementary Table 1.

2.6. Mitochondrial isolation

Cardiac mitochondria were isolated by different centrifugation from male WT and *Atpaf1*-KO mice (15–18 W), as previously described (Huang et al., 2017; Kilbaugh et al., 2015). Briefly, fresh heart tissue was minced and gently homogenized on ice in buffer A (250 mM sucrose, 10 mM Tris/Cl, 0.5 mM EDTA, pH7.4) using a 2 ml Potter-Elvehjem Teflon-glass homogenizer. The homogenate was centrifuged at 800g for 10 min at 4 °C and the supernatant was centrifuged at 8000g for 5 min at 4 °C. The precipitate was washed once again at 8000g for 5 min at 4 °C and the mitochondrial enriched sediments were resuspended in buffer Miro5 (0.5 mM EGTA, 3 mM $MgCl_2{\cdot}6H_2O$, 60 mM K-lactobionate, 20 mM Taurine, 10 mM KH_2PO_4, 20 mM HEPES, 110 mM Sucrose, 1g/L BSA, PH7.1) for 60–100 μl per sample. The protein concentration was determined by the BCA assay (Boster Biological Tech, Wuhan, China).

2.7. Mitochondrial ATP synthase activity

Frozen cardiac mitochondria from −80 °C were thawed on ice to report and the protein concentration was adjusted to 0.6 μg/μl. The mitochondrial ATP hydrolysis (ATPase) activity was measured at 37 °C using a coupled assay to monitor the oxidation of NADH at 340 nm by pyruvate kinase and lactic dehydrogenase reactions, as described previously (Zheng and Ramirez, 1999). The reaction was started by addition of the mitochondria suspension (6 μg/10 μl/well) to a reaction mixture containing a final volume of 90 μl: 100 mM Tris (pH8.0), 4 mM MgATP, 2 mM $MgCl_2$, 50 mM KCl, 0.2 mM EDTA, 0.4 mM NADH, 1 mM phosphoenol pyruvate, 0.2 unit of pyruvate kinase, 0.2 unit of lactate dehydrogenase.

2.8. Assessment of mitochondrial respiration

Respiration of cardiac mitochondria was measured by high-resolution respirometry using the Oxygraph-2 k (OROBOROS INSTRUMENTS, Innsbruck, Austria) at 37 °C (Long et al., 2019). Fresh mitochondrial proteins (100 μg) in air-saturated Miro5 (0.5 mM EGTA, 3 mM $MgCl_2{\cdot}6H_2O$, 60 mM K-lactobionate, 20 mM Taurine, 10 mM KH_2PO_4, 20 mM HEPES, 110 mM Sucrose, 1 g/L BSA, pH7.1) were added to the 2 ml glass chamber (Huang et al., 2017; Kilbaugh et al., 2015). First, malate (2 mM) and pyruvate (5 mM) were added to establish routine mitochondrial respiration, followed by ADP (1 mM) and glutamate (10 mM) to measure the oxidative phosphorylation capacity of complex I(CI). Succinate (10 mM) was subsequently added to stimulate the maximal physiological capacity, complex I and complex II (CII). Thereafter, inhibitors for the different mitochondrial respiratory complexes were added to the chamber in the following order: (1) oligomycin (2μg/ml) to inhibit complex V(CV) (to estimate the overall mitochondrial related respiration), (2) carbonyl cyanide p-(trifluoromethoxy) phenylhydrazone (FCCP) uncoupler with step-wise titration in 0.5 μM increments(to assess maximal electron transport system respiratory capacity rate), and finally (3) rotenone in 0.5 μM final concentration and antimycin A in 2.5 μM final concentration (to measure the non-mitochondrial oxygen consumption) to inhibit complex I and complex III(CIII) respectively.

2.9. Electron microscopy

Mice heart ultrastructural analyses were performed to evaluate mitochondrial structure and function. Hearts from 15 to 18 W mice were perfused and a small piece of myocardium was taken from the LV and fixed in 2.5% glutaraldehyde, then treated with standard dehydration and dyeing processes (Santulli et al., 2015). Sections were examined at different magnifications with an HT7700 transmission electron microscope (HITACHI, Japan). The volume density of mitochondria (Vvm) and the surface density of cristate mitochondria were analyzed as described previously (Drexler et al., 1992; Nielsen et al., 2017).

2.10. BN-PAGE

Blue native PAGE (BN-PAGE) was used for one-step isolation of protein complexes from biological membranes and total cell and tissue homogenates (Wittig et al., 2006) using a protocol as described previously (Beutner and Porter, 2017; Wittig et al., 2006). Every 400μg cardiac mitochondria of mice was suspended in 40 μl solubilization buffer A (50 mM sodium chloride, 50 mM Imidazole/HCL, 2 mM 6-Aminohexanoic acid, 1 mM EDTA, pH7.0) before adding 12 μl detergent, digitonin (20%) and incubated for 10 min on ice. The optimal ratio between protein and digitonin of 6 g/g was used. The sample was centrifuged at 20000g for 20 min at 4 °C. The collected supernatant was supplemented with 5 μl 50% glycerol and 6 μl 5% Coomassie blue G-250 dye, and 10 μl–20 μl each was loaded onto a 4–16% gradient native gel. The electrophoresis conditions were as follows: use cathode buffer B (50 mM tricine, 7.5 mM imidazole, 0.02% Coomassie blue G-250, pH7.0) and set Change cathode buffer B to slightly blue cathode buffer B/10(50 mM tricine, 7.5 mM imidazole, 0.002% Coomassie blue G-250, pH7.0) for better detection for protein bands after the blue running front had moved about one-third of the total running distance. In-gel ATPase activity assay was performed following BN-PAGE (Beutner and Porter, 2017). BN gel can then be fixed and silver stained using a protocol for staining of tricine-SDS gels (Schägger, 2006). 2D BN-PAGE was performed followed by 1D BN-PAGE. Excise a 0.5-cm-wide lane from 1D BN gel, rinse the strip for several seconds with water and load the gel(lane) strip on a tricine-SDS-PAGE by which subunits of the native complexes were separated.

2.11. In-gel ATPase activity assay

In-gel activity ATPase assay was to measure ATP hydrolysis activity as described previously (Yang et al., 2017). The complete BN gel was cut down and immediately soaked in assay buffer (35 mM Tris/Cl, 270 mM glycine, 14 mM $MgSO_4$, 0.2%(w/v) Pb $(NO_3)_2$, 8mM ATP, pH 8.3) at varying time courses. Gels were fixed in 50% methanol and washed in ddH_2O and then scanned. We measured the total white precipitate of three bands (dimer, monomer and free F1) based on densitometry. VDAC was used as a loading control to ensure the same protein loading between WT and *Atpaf1*-KO.

2.12. Detection of ROS production

ROS production was estimated by oxidation of DHE and ratiometric assessment. The frozen heart sections of WT and *Atpaf1*-KO mice were stained with 5 μM DHE and incubated in a light-protected humidified chamber at 37 °C for 30 min. The percentage of DHE-positive nuclei was calculated from fluorescence images with the ImageJ software.

2.13. Histological analysis

Mice were anesthetized with 1% sodium pentobarbital and then killed. The heart was excised, briefly washed in iced PBS and fixed in 4% paraformaldehyde at room temperature for 2 h and stored at 4 °C. Heart samples were embedded in paraffin and processed for histology. WGA, HE and Masson's trichrome staining were performed according to standard procedures and analyzed for the extent of fibrosis and cardiomyocyte cross-sectional area.

2.14. Apoptosis detection by TUNEL assay

A TUNEL assay was performed to evaluate cell apoptosis in myocardial tissues according to the manufacturer's instructions. The nuclei that stained red were considered TUNEL-positive cells. Four fields per slide in each section were chosen randomly to count the number of positive cells at 400× magnification. The apoptosis index (AI) was determined as follows: AI = (the number of positive cells/the total number of counted cells) × 100%.

2.15. Western blotting

The frozen cardiac tissues were lysed in a RIPA buffer (Wuhan Servicebio Tech, Wuhan, China) with PMSF, protease inhibitor and phosphatase inhibitor (Boster Biological Tech, Wuhan, China) according to manufacturer's instructions. Myocardial homogenates were collected from the supernatant after centrifugation at 12000g at 4 °C for 15 min. Protein concentrations were measured with the BCA Protein Assay Kit (Boster Biological Tech, Wuhan, China) using a spectrophotometer. An equal amount of proteins (20μg for myocardial homogenates) for each sample were size-separated by 10–12% SDS-PAGE gel electrophoresis and transferred to a PVDF membrane (EMD Millipore, Billerica, MA, USA), and blocked with 5% nonfat dye milk for 2 h at room temperature. The membrane was incubated with primary antibodies at 4 °C overnight followed by incubation with horseradish peroxidase-conjugated secondary antibody at room temperature for 2 h and visualized using the ECL western blotting detection reagent (Vazyme Biotech, Nanjing, China). Equivalent protein loads were verified and normalized by GAPDH (1:1000, Wuhan Servicebio Tech, Wuhan, China) blots. Finally, bands were analyzed by ImageJ software. Primary antibodies were as follows: ATPAF1 (1:1000, Santa Cruz Biotechnology, CA, US), ATP5A (1:1000, ABclonal Biotechnology, Wuhan, China), ATP5B (1:1000, ABclonal Biotechnology, Wuhan, China), VDAC (1:1000, ABclonal Biotechnology, Wuhan, China), Caspase3 (1:1000, Cell Signaling Tech, MA, US), cleaved Caspase3 (1:1000, Cell Signaling Tech, MA, US). LC3 (1:1000, ABclonal Biotechnology, Wuhan, China), MFN1 (1:1000, ABclonal Biotechnology, Wuhan, China), MFN2 (1:1000, ABclonal Biotechnology, Wuhan, China), OPA1 (1:1000, ABclonal Biotechnology, Wuhan, China), DRP1 (1:1000, ABclonal Biotechnology, Wuhan, China), CI-NDUFB8 (1:1000, ABclonal Biotechnology, China) CII-SDHB (1:1000, ABclonal Biotechnology, China), CIII-UQCRC2 (1:1000, ABclonal Biotechnology, China), CIV-MTCO1 (1:1000, ABclonal Biotechnology, China); Horseradish peroxidase (HRP) linked secondary antibodies anti-mouse IgG (1:5000) and anti-rabbit IgG (1:5000) were from Boster Biological Tech, Wuhan, China.

2.16. Statistical analyses

Data were analyzed using the nonparametric Student *t*-test for two-group comparisons; otherwise, data were analyzed by one-factor or mixed, two-factor ANOVA and multiple comparisons test. Data were presented as mean ± SEM unless otherwise indicated in figure legends. $p < 0.05$ was considered statistically significant.

3. Results

3.1. Mice with homozygous Atpaf1 knockout are viable with decreased body weight.

To investigate the *in vivo* role of ATPAF1 and ATPAF2 in ATP synthase assembly and the pathophysiological consequences, we generated mice with *Atpaf1* and *Atpaf2* deficiencies using the CRISPR/Cas9 technology (Cyagen Biosciences (Suzhou) Inc.). We have obtained F1 pups of *Atpaf1* and *Atpaf2* with heterozygous KO (Fig. 1A, B). While no pups with homozygous *Atpaf2*-KO were born, we obtained homozygous *Atpaf1* knockout mice with normal litter size. The mRNA expression of *Atpaf1* was assessed using semi-quantitative RT-PCR which indicated no detection of *Atpaf1* at the transcript level (Fig. 1C). Western blots on samples extracted from the heart, brain, liver, and skeletal muscle confirm that the ATPAF1 allele was deleted (Fig. 1D). The lack of *Atpaf1* does not affect the breeding or development of mice. The *Atpaf1*-KO mice did not show overt signs of behavioral abnormalities. The *Atpaf1*-KO mice (male and female) grew slower than wild type mice with modestly reduced body weight (Fig. 1E) for the first half year, also, the knockout mice did not recover to similar body weight as the wildtype littermates after 6 months. Plasma lactate contents were initially unchanged and arose in *Atpaf1*-KO mice reached their age of 25–30 weeks compared with WT mice (Fig. 1F). These results suggest that *Atpaf1*, unlike *Atpaf2*, is not essential for embryonic development, but its deficiency leads to growth retardation and lactatemia respectively in young and adult mice.

3.2. ATPAF1 interacts with the β-subunit of ATP synthase

We confirmed that ATPAF1 was co-localized with the mitochondrial β-subunit ATP5B via immunofluorescence staining, which was consistent with previous studies (Saito et al., 2010) (Fig. 2A). Moreover, previous studies show that Atp11p binds to the β-subunit in yeast (Wang and Ackerman, 2000). To confirm a similar binding in mammalian cells, we performed Co-IP experiments in WT HEK293 cells with *Atpaf1* transient overexpression (Supplementary S3. A). Co-IP experiments showed that the endogenous β-subunit interacts with ATPAF1 (Fig. 2B). We next investigated whether ATPAF1 deficiency affects the assembly of ATP synthase. We examined cardiac ATP5A (α-subunit) and ATP5B (β-subunit) expression in wild type and *Atpaf1* deficient hearts using Western blot on mitochondrial protein extracts. Both the expression of α- and β-subunits were decreased in mitochondrial proteins from *Atpaf1*-KO compared with WT mouse hearts (Fig. 2C-E). Protein abundances of other respiratory chain complexes in *Atpaf1*-KO hearts were comparable with those of WT mice (Supplementary S2. A-B). These data demonstrate that ATPAF1 is essential to maintain the normal abundance of α- and β-subunits of the F1 component of ATP synthase. The lack of ATPAF1 appears to impair F1 assembly.

3.3. Absence of ATPAF1 reduces ATP synthase, dimerization, and activity

We next conducted immunoblots on protein samples transferred from BN-PAGE to detect ATP synthase F1 in dimeric, monomeric, and free F1 forms (Fig. 3A, B). The relative expression of dimeric and monomeric F1 in *Atpaf1*-KO hearts was markedly reduced compared with the WT control (Fig. 3C). Two-dimensional BN-PAGE (2D BN-PAGE) revealed a reduced ATP synthase content in the *Atpaf1*-KO compared to the WT hearts (Fig. 3D; Supplementary S.3B). Furthermore, In-gel ATPase staining showed a 40–65% decrease in ATPase activity in mitochondria extracted from *Atpaf1*-KO vs WT hearts (Fig. 3E, F; Supplementary S4 D and E). The biochemical assay showed that the *Atpaf1*-deficient hearts had a decreased ATP synthase (ATPase) activity compared with WT control hearts (Fig. 3G, H). Therefore, these results indicate that the loss of ATPAF1 will lead to reduced ATP synthase activity and dimerization due to its role in assembling ATP synthase F1.

3.4. Deficiency of Atpaf1 attenuates mitochondrial respiration capacities, resulting in increased ROS generation, mitochondrial depolarization and disrupting mitochondrial morphology

The functional effects of *Atpaf1* deficiency on mitochondrial energy conversion were analyzed using a high-resolution Oroboros Oxygraph system. Specifically, routine mitochondrial respiration was measured via the concomitant addition of malate and pyruvate, followed by ADP and glutamate representing oxidative phosphorylation (OXPHOS) capacity of CI ($OXPHOS_{CI}$), driven by the NADH-related substrates. Succinate was added to stimulate maximal OXPHOS capacity ($OXPHOS_{CI+CII}$). All these three capacities were reduced in mitochondria extracted from *Atpaf1*-KO compared with WT hearts (Fig. 4A-C), whereas LEAK respiration ($LEAK_{CI+CII}$), mitochondrial respiration independent of ATP-production, and the maximal convergent non-phosphorylating respiration of the electron transport system (ETS_{CI+CII}) were not altered (Fig. 4D, E). Subsequently, rotenone was added to inhibit CI to measure the electron transport system (ETS) capacity supported by succinate alone through CII(ETS_{CII}). Finally, electron flow through the ETS was blocked by the complex III(CIII) inhibitor antimycin-A (AA), revealing the residual oxygen consumption not related to ETS. This value was subtracted from every respiratory state in the analysis. Furthermore, we analyzed the respiratory control ratios (RCR) (Fig. 4F) to evaluate the structural integrity of the inner mitochondrial membrane (IMM) and OXPHOS efficiency. In-gel CI-CIV activity staining on BN-PAGE gels showed that a reduced CI activity in samples from *Atpaf1*-KO compared with WT hearts (Supplementary S2. C-F). Furthermore, DHE staining for superoxide was increased in *Atpaf1*-KO compared with those of WT heart sections (Fig. 4G, H). In addition, the relative expression of the superoxide related gene was detected by qPCR (Supplementary S3. C-F). The NADPH oxidase subunit NOX4, a substrate of NADPH that can generate ROS, was increased in *Atpaf1*-KO group. While the relative expression of *Gpx1* which encodes GPX1, a member of the antioxidant enzyme system was decreased in *Atpaf1*-KO. We next assessed the rate of calcium induced mitochondrial permeability transition (MPT) pore activation and found no change (Fig. 4I). We further investigate how mitochondrial quality control and dynamic changes in response to the observed mitochondrial dysfunction caused by *Atpaf1* deficiency. As a marker of autophagosome membranes, changes in cellular LC3-II level are connected to autophagic activity. DRP1-mediated mitochondrial fission,

OPA1, MFN-mediated mitochondrial fusion maintain mitochondrial dynamism. Western blots revealed that LC3 II protein was downregulated in *Atpaf1*-KO relative to WT control (Fig. 5 A, B). Whereas western blot detected no change of mitofusin 1 (MFN1) protein (Fig. 5C, D), the protein abundances of Optic atrophy 1 (OPA1) and mitofusin 2 (MFN2) were decreased and dynamin-related protein 1 (DRP1) were increased in the *Atpaf1*-KO compared with WT group (Fig. 5E-G), suggesting imbalanced mitochondrial autophagy and dynamics may occur in the *Atpaf1*-KO heart. Transmission electron microscopy (TEM) assessment revealed disorganized and smaller mitochondria with reduced cristae density and mitochondria area in *Atpaf1*-KO heart sections compared with those of WT (Fig. 6A-C). Therefore, these results demonstrate that the lack of *Atpaf1* and subsequent ATP synthase deficiency lead to major impacts on mitochondrial homeostasis.

3.5. Deletion of Atpaf1 in mice leads to cardiac dysfunction and LV remodeling

We next investigated how the ATP synthase deficiency and the subsequent mitochondrial defects would impact cardiac structure and function. Echocardiographic assessment at different time points revealed that the *Atpaf1*-KO mice (male) exhibited sustained decrease in ejection fraction (EF%) (Fig. 7A, B) and fractional shortening (FS%) (Fig. 7C), which were similar to those of female mice (Supplementary S4A-C. The *Atpaf1*-KO hearts showed increases in heart weight/tibia length ratio and the relative *Bnp* mRNA expression (Fig. 7D-F). Furthermore, histological examination using HE and WGA staining on heart sections revealed that the cardiomyocyte cross-section area was enlarged in *Atpaf1*-KO compared with WT hearts (Fig. 7G, H). Masson's trichrome staining displayed elevated fibrosis in *Atpaf1*-KO hearts relative to WT hearts (Fig. 7G, I). TUNEL assays revealed that apoptotic cells were increased in *Atpaf1*-KO compared to that of WT hearts (Fig. 8A, B). Western blot analysis revealed that the cleaved Caspase 3 was increased in *Atpaf1*-KO compared with WT hearts (Fig. 8C-E). These results demonstrate that the lack of *Atpaf1* in adult mice caused cardiac dysfunction, hypertrophy and remodeling.

4. Discussion

The assembly of mitochondrial ATP synthase in mammalian cells remains largely a midstory. The present study provides *in vivo* evidence supporting that ATPAF1 is essential for ATP synthase F1 assembly and ATP synthase activity, leading to numerous mitochondria defects and the development of dilated cardiomyopathy. These results uncover for the first time the essential role of ATPAF1-dependent ATP synthase in maintaining the operation of ATP synthase, mitochondrial homeostasis, and organ function.

ATPAF1, a ~31–32-kDa mitochondrial protein, is a nuclear gene product that is required for carrying the β subunit for the assembly of mitochondrial F1-ATP synthase in yeast (Ackerman et al., 1992; Ackerman and Tzagoloff, 1990; White and Ackerman, 1995). In addition to the ATPAF1, ATPAF2, another nuclear gene encoded protein, is thought to be responsible for the assembly of α subunit (Ackerman and Tzagoloff, 1990; Bowman et al., 1991; Wang and Ackerman, 1998). In this study, we generated F1 pups of both ATPAF1 and ATPAF2 with heterozygous KO. Unlike germline transmission of ATPAF1 heterozygotes, no viable pups with homozygous *Atpaf1*-KO were born. The global KO *Atpaf2* mice generated

using another strategy also showed preweaning lethality (EuMMCR/EMMA Repository). This observation illustrates the essential requirement of ATP synthase for the early stages of mammalian prenatal development. The results implicate that ATPAF2 may have a more crucial function in the final assembly and the activity of ATP synthase. This observation is consistent with previous studies in yeast, in which more than 60% of ATP synthase activity was lost in *Atpaf2* null yeast and only 30% of ATP synthase activity was lost in *Atpaf1* null yeast (Ackerman and Tzagoloff, 1990). Our result confirm that ATPAF1 interacts with F1 β-subunit as those shown in yeast studies (Wang and Ackerman, 2000). However, we have to overexpress *Atpaf1* in cultured HEK293 cells to detect the interaction. It appears that the F1 assembly event is minimal under basal condition. However, the loss of ATPAF1 is sufficient to impair F1 assembly. Moreover, both the expression of α- and β-subunits were decreased in mitochondrial proteins from Atpaf1-KO mouse. As the main structure protein in F1 domain, the α- and β-subunits together form a (αβ)3 subcomplex, indicating that loss of ATPAF1 impacted alpha subunit indirectly. Meanwhile, we could also speculate that the role of ATPAF1 is binding and protecting ATP5B stability and loss causes loss of ATP5B stability, which then because of the stoichiometry of the enzyme causing secondary degradation of ATP5A. Therefore, the *Atpaf1*-KO mice provide an ideal model to gain insights into the role of ATP synthase assembly in animal cells and tissues.

The biogenesis of ATP synthase is a complicated process depending on different ancillary factors. At least 13 ATP synthase -specific factors exist in yeast, but only limiting factors related to mammalian ATP synthase have been found so far (Havlíčková et al., 2010). The identification of conserved metallopeptidase called ATP23 mediates the maturation of the mitochondrial-encoded Fo-subunit atp6 (Osman et al., 2007). TMEM70 was suggested as a novel factor of ATP synthase biogenesis in eukaryotes (Hejzlarová et al., 2011; Kratochvílová et al., 2014). In addition to ATPAF1, ATPAF2 is thought to be responsible for the assembly of α subunit (Ackerman and Tzagoloff, 1990; Wang and Ackerman, 1998). Our results demonstrate that the feasibility of using molecular genetic approach to preclinical animal models gained novel insights into the sequential biochemical and pathological mechanisms, which may lead to better therapeutic options for the treatment of ATP synthase deficiencies and to cardiac disorders in general.

ATP synthase catalyzes the synthesis of ATP from ADP and inorganic phosphate utilizing the energy of an electrochemical ion gradient. In contrast, ATP synthase function as ATPase (ATP hydrolysis) under conditions of low driving force, exiting in the hydrolysis process (Deckers-Hebestreit and Altendorf, 1996). In *Atpaf1*-KO mouse hearts, the defect manifested functionally as a pronounced decrease in ATP synthase activity. In addition, respiratory capacity of isolated mitochondria from *Atpaf1*-KO mouse heart was impaired. Despite no differences in the LEAK respiration (mitochondrial respiration independent of ATP production) and maximal convergent respiratory capacity of the electron transport system, *Atpaf1*-KO mice displayed lower efficiency in basal respiration and oxidative phosphorylation capacity of both CI and CII as compared to WT mice, indicating the impaired mitochondrial function in *Atpaf1* deficiency mice. However, further studies will require to determine if the ATP synthase deficiency in the *Atpaf1*-KO heart impairs mitochondrial respiration directly or indirectly via mitochondrial morphological defects.

Cristae formation extends the membrane surface to accommodate the respiratory chain complexes, making it possible to meet the high energy demands of eukaryotic cells (Lane and Martin, 2010). An interesting finding of our study is that the deletion of *Atpaf1* in adult mice affects the content and dimerization of ATP synthase, supporting indirectly the hypothesis that mitochondrial ATP synthase plays a role in forming dimeric arrays in the inner membrane of yeast and mammalian mitochondria (Campanella et al., 2008; Hahn et al., 2016). Our experiments based on BN-PAGE and the following western blots to separate the respiratory chain complexes demonstrate that the dimer, monomer, and free F1 of the ATP synthase in mitochondria of *Atpaf1*-KO mouse hearts were all decreased. ATP synthase dimerization is involved in shaping the mitochondrial cristae and thus the biogenesis of the inner mitochondrial membrane (Davies et al., 2012; Paumard et al., 2002; Strauss et al., 2008). As an assembly factor for ATP synthase, the deletion of *Atpaf1* reduces the dimerization content of ATP synthase, thus altering the structure and density of mitochondria, which is evident by the ultrastructural changes in the *Atpaf1*-KO heart with vacuolization, swelling, and loss of mitochondrial cristae.

Mitochondria are the main source of endogenous reactive oxygen species (ROS) (Murphy and Steenbergen, 2007) which drives oxidative stress and causes cellular dysfunction and damage at higher levels (Peoples et al., 2019; Pohjoismäki and Goffart, 2017; Tsutsui et al., 2011). The observed cardiac dysfunction and pathology in the *Atpaf1*-KO heart should also be derived from excessive ROS production due to the inefficient oxidative phosphorylation. The increased oxidative stress is apparently contributing to the modest depolarization of the mitochondria. However, oxidative stress appears within a tolerated level to not trigger the opening of MPTP. Taken together, inefficient oxidative phosphorylation, ATP deficit and mitochondrial defects due to loss of cristae density and increased ROS in the *Atpaf1*-KO mice may all contribute to cardiac cell death, following cardiac dysfunction, dilated hypertrophy and remodeling. Despite the dramatic impairment of mitochondrial structure and function, autophagy and mitochondrial dynamics in *Atpaf1*-KO mice were also impaired. However, the mechanisms underlying the dysregulation autophagy and potential upregulation of mitochondrial fission are not clear, but plausibly related to energy depletion and mal-adaptation to the ATP synthase deficiency.

Patients with severe ATP synthase deficiencies or mitochondrial dysfunction often manifest cardiac defects, which lead to early death (Malfatti et al., 2013; Mráček et al., 2006). *Atpaf1*-KO mice showed early and sustained cardiac dysfunction, dilatation, and remodeling, but mostly survival through adulthood, indicating that *Atpaf1*-KO-related ATP synthase deficiency is relatively modest and not progressive. *Atpaf1*-KO mice, as a preclinical model, will provide an unprecedented opportunity for in-depth investigations to understand the biochemical and pathological mechanisms for better care and prevention among patients with partial ATP synthase deficiencies. The impairment of ATP synthase activity in *Atpaf1* null mice appear relatively modest but sufficient to cause cardiac phenotype in the heart, which is an organ with high demands on mitochondrial oxidative energy (Bindoff, 2003; Limongelli et al., 2017). The adverse consequences of cardiac dysfunction and LV remodeling in the *Atpaf1*-KO mice suggest that ATPAF1 is essential for the mouse to maintain normal heart function. However, the phenotypic changes in the heart could partly be derived from global metabolic changes. Future studies using tissue-specific

gene targeting animals should help gain crucial insights into the role of ATPAF1 in cardiac pathophysiology.

5. Conclusion

In summary, results from the present investigation on a preclinical mouse model of *Atpaf1*-KO provide strong support that ATPAF1 is essential for ATP synthase assembly, mitochondrial morphology, and oxidative phosphorylation, thus playing a crucial role in maintaining cardiac structure and function.

Supplementary Material

Refer to Web version on PubMed Central for supplementary material.

Funding

This work was supported by grants from the National Natural Science Foundation of China (81500312) and American Heart Association (AHA) Post-doctoral Fellowship (13POST14180006) to QL, American Diabetes Association (ADA) (1-17-IBS-184) and National Institutes of Health (NIH) (R01HL13533) to QY. The funding sponsors played no role in study design, data collection and analysis, interpretation, writing of the report, and the decision to submit the paper for publication.

Abbreviations:

ATPAF1	ATP synthase mitochondrial F1 complex assembly factor 1
ATPAF2	ATP synthase mitochondrial F1 complex assembly factor 2
LV	left ventricle
KO	knockout
WT	wild type
BN-PAGE	Blue-Native electrophoresis
FCCP	carbonyl cyanide p-(trifluoromethoxy) phenylhydrazone
2D BN-PAGE	two-dimensional BN-PAGE
TEM	transmission electron microscopy
OXPHOS	oxidative phosphorylation
CI	complex I
CII	complex II
CIII	complex III
CIV	complex IV
CV	complex V
ETS	the electron transport system

RCR	the respiratory control ratios
AA	antimycin-A
IMM	the inner mitochondrial membrane
Anp/Nppa	natriuretic peptide type A
Bnp/Nppb	natriuretic peptide type B
MPT	mitochondrial permeability transition
MFN1	mitofusin1
MFN2	mitofusion2
OPA1	Optic atrophy 1
L-OPA1	long form of OPA1
S-OPA1	short form of OPA1
DRP1	dynamin-related protein1
LC3	microtubule-associated protein light chain 3
Gal4p	galactose-responsive transcription factor
Gpx1	glutathione peroxidase1
Nox4	NADPH oxidase 4
Sod1	superoxide dismutase 1
Sod2	superoxide dismutase 2

References

Ackerman SH, Martin J, Tzagoloff A, 1992. Characterization of ATP11 and detection of the encoded protein in mitochondria of Saccharomyces cerevisiae. J. Biol. Chem 267 (11), 7386–7394. [PubMed: 1532796]

Ackerman SH, Tzagoloff A, 1990. Identification of two nuclear genes (ATP11, ATP12) required for assembly of the yeast F1-ATPase. Proc. Natl. Acad. Sci. U.S.A 87 (13), 4986–4990. [PubMed: 2142305]

Artika IM, 2019. Current understanding of structure, function and biogenesis of yeast mitochondrial ATP synthase. J. Bioenerg. Biomembr 51 (5), 315–328. [PubMed: 31418131]

Beutner G, Porter GA, 2017. Analyzing supercomplexes of the mitochondrial electron transport chain with native electrophoresis, in-gel assays, and electroelution. J. Vis. Exp (124), 55738. 10.3791/55738, . [PubMed: 28605384]

Bindoff L, 2003. Mitochondria and the heart. Eur. Heart J 24 (3), 221–224. [PubMed: 12590900]

Bowman S, Ackerman SH, Griffiths DE, Tzagoloff A, 1991. Characterization of ATP12, a yeast nuclear gene required for the assembly of the mitochondrial F1-ATPase. J. Biol. Chem 266 (12), 7517–7523. [PubMed: 1826907]

Campanella M, Casswell E, Chong S, Farah Z, Wieckowski MR, Abramov AY, Tinker A, Duchen MR, 2008. Regulation of mitochondrial structure and function by the F1Fo-ATPase inhibitor protein, IF1. Cell Metab. 8 (1), 13–25. [PubMed: 18590689]

Davies KM, Anselmi C, Wittig I, Faraldo-Gomez JD, Kuhlbrandt W, 2012. Structure of the yeast F1Fo-ATP synthase dimer and its role in shaping the mitochondrial cristae. Proc. Natl. Acad. Sci. U.S.A 109 (34), 13602–13607. [PubMed: 22864911]

De Meirleir L, Seneca S, Lissens W, De Clercq I, Eyskens F, Gerlo E, Smet J, Van Coster R, 2004. Respiratory chain complex V deficiency due to a mutation in the assembly gene ATP12. J. Med. Genet 41, 120–124. [PubMed: 14757859]

de Vries DD, van Engelen BGM, Gabreëls FJM, Ruitenbeek W, van Oost BA, 1993. A second missense mutation in the mitochondrial ATPase 6 gene in Leigh's syndrome. Ann. Neurol 34 (3), 410–412. [PubMed: 8395787]

Deckers-Hebestreit G, Altendorf K, 1996. The F0F1-type ATP synthases of bacteria: structure and function of the F0 complex. Annu. Rev. Microbiol 50 (1), 791–824. [PubMed: 8905099]

Drexler H, Riede U, Münzel T, König H, Funke E, Just H, 1992. Alterations of skeletal muscle in chronic heart failure. Circulation 85 (5), 1751–1759. [PubMed: 1315220]

Ghezzi D, Zeviani M, 2018. Human diseases associated with defects in assembly of OXPHOS complexes. Essays Biochem. 62 (3), 271–286. [PubMed: 30030362]

Hahn A, Parey K, Bublitz M, Mills D, Zickermann V, Vonck J, Kühlbrandt W, Meier T, 2016. Structure of a complete ATP synthase dimer reveals the molecular basis of inner mitochondrial membrane morphology. Mol. Cell 63 (3), 445–456. [PubMed: 27373333]

Havlíčková V, Kaplanová V, Nůsková H, Drahota Z, Houštěk J, 2010. Knockdown of F1 epsilon subunit decreases mitochondrial content of ATP synthase and leads to accumulation of subunit c. BBA 1797 (6-7), 1124–1129. [PubMed: 20026007]

Hejzlarová K, Tesařová M, Vrbacká-Čížková A, Vrbacký M, Hartmannová H, Kaplanová V, Nosková L, Kratochvílová H, Buzková J, Havlíčková V, Zeman J, Kmoch S, Houštěk J, 2011. Expression and processing of the TMEM70 protein. BBA 1807 (1), 144–149. [PubMed: 20937241]

Hong S, Pedersen PL, 2008. ATP synthase and the actions of inhibitors utilized to study its roles in human health, disease, and other scientific areas. Microbiol. Mol. Biol. Rev 72 (4), 590–641. [PubMed: 19052322]

Huang L, Zhang K, Guo Y, Huang F, Yang K, Chen L, Huang K, Zhang F, Long Q, Yang Q, 2017. Honokiol protects against doxorubicin cardiotoxicity via improving mitochondrial function in mouse hearts. Sci. Rep 7, 11989. [PubMed: 28931882]

Kabaleeswaran V, Puri N, Walker JE, Leslie AGW, Mueller DM, 2006. Novel features of the rotary catalytic mechanism revealed in the structure of yeast F1 ATPase. EMBO J. 25 (22), 5433–5442. [PubMed: 17082766]

Kilbaugh TJ, Karlsson M, Byro M, Bebee A, Ralston J, Sullivan S, Duhaime A-C, Hansson MJ, Elmér E, Margulies SS, 2015. Mitochondrial bioenergetic alterations after focal traumatic brain injury in the immature brain. Exp. Neurol 271, 136–144. [PubMed: 26028309]

Kratochvílová H, Hejzlarová K, Vrbacký M, Mráček T, Karbanová V, Tesařová M, Gombitová A, Cmarko D, Wittig I, Zeman J, Houštěk J, 2014. Mitochondrial membrane assembly of TMEM70 protein. Mitochondrion 15, 1–9. [PubMed: 24576557]

Lane N, Martin W, 2010. The energetics of genome complexity. Nature 467 (7318), 929–934. [PubMed: 20962839]

Limongelli G, Masarone D, Pacileo G, 2017. Mitochondrial disease and the heart. Heart 103 (5), 390–398. [PubMed: 27821705]

Long Q, Huang L, Huang K, Yang Q, 2019. Assessing mitochondrial bioenergetics in isolated mitochondria from mouse heart tissues using oroboros 2k-oxygraph. Methods Mol. Biol 1966, 237–246. [PubMed: 31041752]

Malfatti E, Laforet P, Jardel C, Stojkovic T, Behin A, Eymard B, Lombes A, Benmalek A, Becane HM, Berber N, Meune C, Duboc D, Wahbi K, 2013. High risk of severe cardiac adverse events in patients with mitochondrial m.3243A>G mutation. Neurology 80, 100–105. [PubMed: 23243073]

Mráček T, Pecina P, Vojtíšková A, Kalous M, Šebesta O, Houštěk J, 2006. Two components in pathogenic mechanism of mitochondrial ATPase deficiency: energy deprivation and ROS production. Exp. Gerontol 41 (7), 683–687. [PubMed: 16581217]

Murphy E, Steenbergen C, 2007. Preconditioning: the mitochondrial connection. Annu. Rev. Physiol 69 (1), 51–67. [PubMed: 17007587]

Nakamoto RK, Baylis Scanlon JA, Al-Shawi MK, 2008. The rotary mechanism of the ATP synthase. Arch. Biochem. Biophys 476 (1), 43–50. [PubMed: 18515057]

Nielsen J, Gejl KD, Hey-Mogensen M, Holmberg H-C, Suetta C, Krustrup P, Elemans CPH, Ørtenblad N, 2017. Plasticity in mitochondrial cristae density allows metabolic capacity modulation in human skeletal muscle. J. Physiol 595 (9), 2839–2847. [PubMed: 27696420]

Osman C, Wilmes C, Tatsuta T, Langer T, Fox T, 2007. Prohibitins interact genetically with Atp23, a novel processing peptidase and chaperone for the F1Fo-ATP synthase. Mol. Biol. Cell 18 (2), 627–635. [PubMed: 17135288]

Paumard P, Vaillier J, Coulary B, Schaeffer J, Soubannier V, Mueller DM, Brethes D, di Rago JP, Velours J, 2002. The ATP synthase is involved in generating mitochondrial cristae morphology. EMBO J. 21, 221–230. [PubMed: 11823415]

Peoples JN, Saraf A, Ghazal N, Pham TT, Kwong JQ, 2019. Mitochondrial dysfunction and oxidative stress in heart disease. Exp. Mol. Med 51 (12), 1–13.

Pohjoismäki JL, Goffart S, 2017. The role of mitochondria in cardiac development and protection. Free Radic. Biol. Med 106, 345–354. [PubMed: 28216385]

Saito K, Adachi N, Koyama H, Matsushita M, 2010. OGFOD1, a member of the 2-oxoglutarate and iron dependent dioxygenase family, functions in ischemic signaling. FEBS Lett. 584, 3340–3347. [PubMed: 20579638]

Santulli G, Xie W, Reiken SR, Marks AR, 2015. Mitochondrial calcium overload is a key determinant in heart failure. Proc. Natl. Acad. Sci. U.S.A 112 (36), 11389–11394. [PubMed: 26217001]

Schägger H, 2006. Tricine-SDS-PAGE. Nat. Protoc 1 (1), 16–22. [PubMed: 17406207]

Srivastava AP, Luo M, Zhou W, Symersky J, Bai D, Chambers MG, Faraldo-Gómez JD, Liao M, Mueller DM, 2018. High-resolution cryo-EM analysis of the yeast ATP synthase in a lipid membrane. Science 360 (6389). 10.1126/science:aas9699, 29650704.

Stock D, Gibbons C, Arechaga I, Leslie AGW, Walker JE, 2000. The rotary mechanism of ATP synthase. Curr. Opin. Struct. Biol 10 (6), 672–679. [PubMed: 11114504]

Strauss M, Hofhaus G, Schröder RR, Kühlbrandt W, 2008. Dimer ribbons of ATP synthase shape the inner mitochondrial membrane. EMBO J. 27 (7), 1154–1160. [PubMed: 18323778]

Tsutsui H, Kinugawa S, Matsushima S, 2011. Oxidative stress and heart failure. Am. J. Physiol. Heart Circ. Physiol 301 (6), H2181–H2190. [PubMed: 21949114]

Wang Z-G, Ackerman SH, 1998. Mutational studies with Atp12p, a protein required for assembly of the mitochondrial F1-ATPase in yeast. Identification of domains important for Atp12p function and oligomerization. J. Biol. Chem 273 (5), 2993–3002. [PubMed: 9446613]

Wang ZG, Ackerman SH, 2000. The assembly factor Atp11p binds to the beta-subunit of the mitochondrial F(1)-ATPase. J. Biol. Chem 275, 5767–5772. [PubMed: 10681564]

Wang Z-G, White PS, Ackerman SH, 2001. Atp11p and Atp12p are assembly factors for the F(1)-ATPase in human mitochondria. J. Biol. Chem 276 (33), 30773–30778. [PubMed: 11410595]

White M, Ackerman SH, 1995. Bacterial production and characterization of ATP11, a yeast protein required for mitochondrial F1-ATPase assembly. Arch. Biochem. Biophys 319 (1), 299–304. [PubMed: 7771799]

Wittig I, Braun H-P, Schägger H, 2006. Blue native PAGE. Nat. Protoc 1 (1), 418–428. [PubMed: 17406264]

Yang K, Long Q, Saja K, Huang F, Pogwizd SM, Zhou L, Yoshida M, Yang Q, 2017. Knockout of the ATPase inhibitory factor 1 protects the heart from pressure overload-induced cardiac hypertrophy. Sci. Rep 7, 10501. [PubMed: 28874825]

Zheng J, Ramirez VD, 1999. Rapid inhibition of rat brain mitochondrial proton F0F1-ATPase activity by estrogens: comparison with Na+, K+ -ATPase of porcine cortex. Eur. J. Pharmacol 368 (1), 95–102. [PubMed: 10096774]

Zhou A, Rohou A, Schep DG, Bason JV, Montgomery MG, Walker JE, Grigorieff N, Rubinstein JL, 2015. Structure and conformational states of the bovine mitochondrial ATP synthase by cryo-EM. Elife 4, e10180. 10.7554/eLife.10180, 26439008. [PubMed: 26439008]

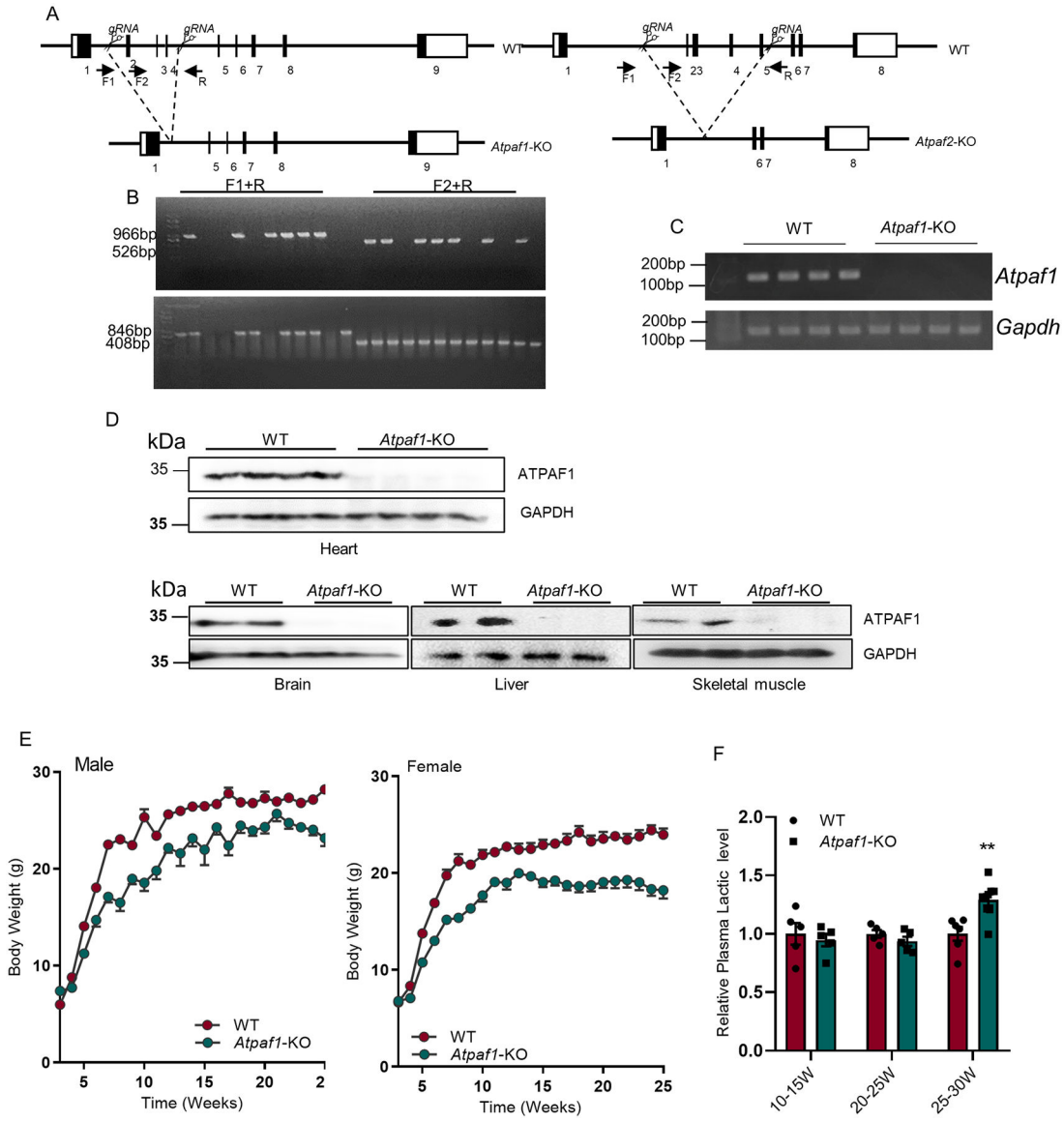

Fig. 1.

ATPAF1 protein expression, plasma lactate content and body weight changes between wild type and *Atpaf1*-KO mice. (A) Scheme for generating the *Atpaf1* and *Atpaf2* knockout mice. F1, F2, R with arrow represent primer information. (B) Genotyping of progeny from *Atpaf1* and *Atpaf2* heterozygous intercross. *Atpaf1*: homozygotes: 966 bp, heterozygotes: 966 bp/526 bp, wildtype allele: 526 bp. *Atpaf2*: homozygotes: 846 bp, heterozygotes: 846 bp/408 bp, wildtype allele: 408 bp. (C) The transcript level of Atpaf1 was assessed using semi-quantitative RT-PCR. (D) Protein levels of ATPAF1 in heart/brain/liver/skeletal muscle tissues were determined by Western blots. GAPDH was used as protein loading control. Samples were extracted from 20 to 25 weeks mice (n = 2–4). (E) Body weight curves of WT and *Atpaf1*-KO mice at different weeks (Male and female mice: 3–25 weeks, n = 5–20). (F) Plasma lactic acid concentration. Red bar chart indicated the WT and the green indicted the

Atpaf1-KO. Samples were taken from mice plasma centrifuged after leaving the blood at 4 °C for 2–4 h (n = 5–8). **p < 0.01 vs wild type. Values are expressed as mean ± SEM.

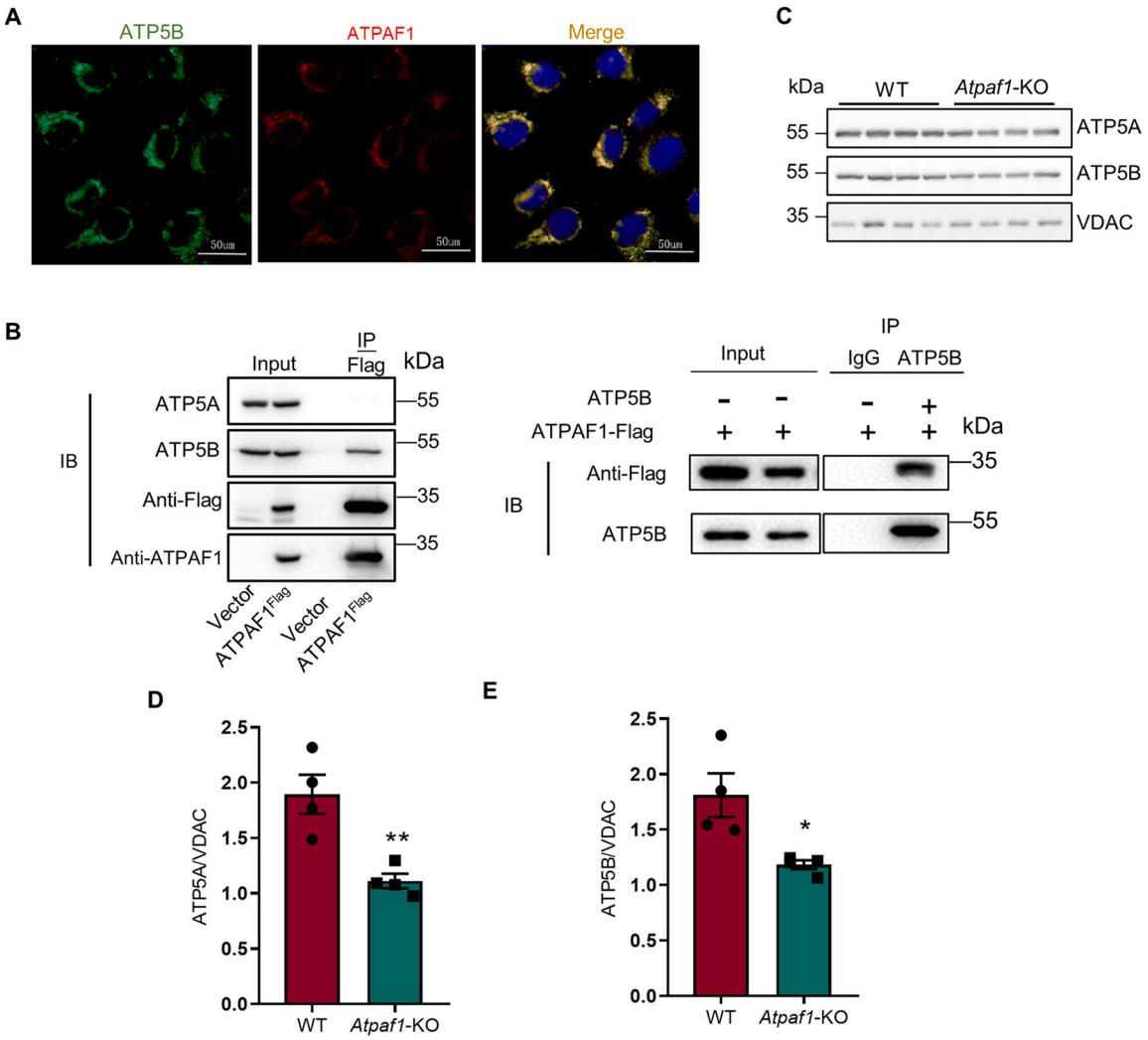

Fig. 2.

ATPAF1 interacts with the β-subunit of ATP synthase. (A) Subcellular localization of ATPAF1 in AC16 cells. (B) Interactions between ATPAF1 and α-, β-subunits. (C) Western blot analysis of ATP5A and ATP5B on mitochondrial protein samples. VDAC was used as the protein loading control. Samples were mitochondrial protein extracted from LV tissue of 20-week mice (n = 4). (D-E) Quantitative analysis of the blots. *$p < 0.05$ vs wild type. **$p < 0.01$ vs wild type. Values are expressed as mean ± SEM.

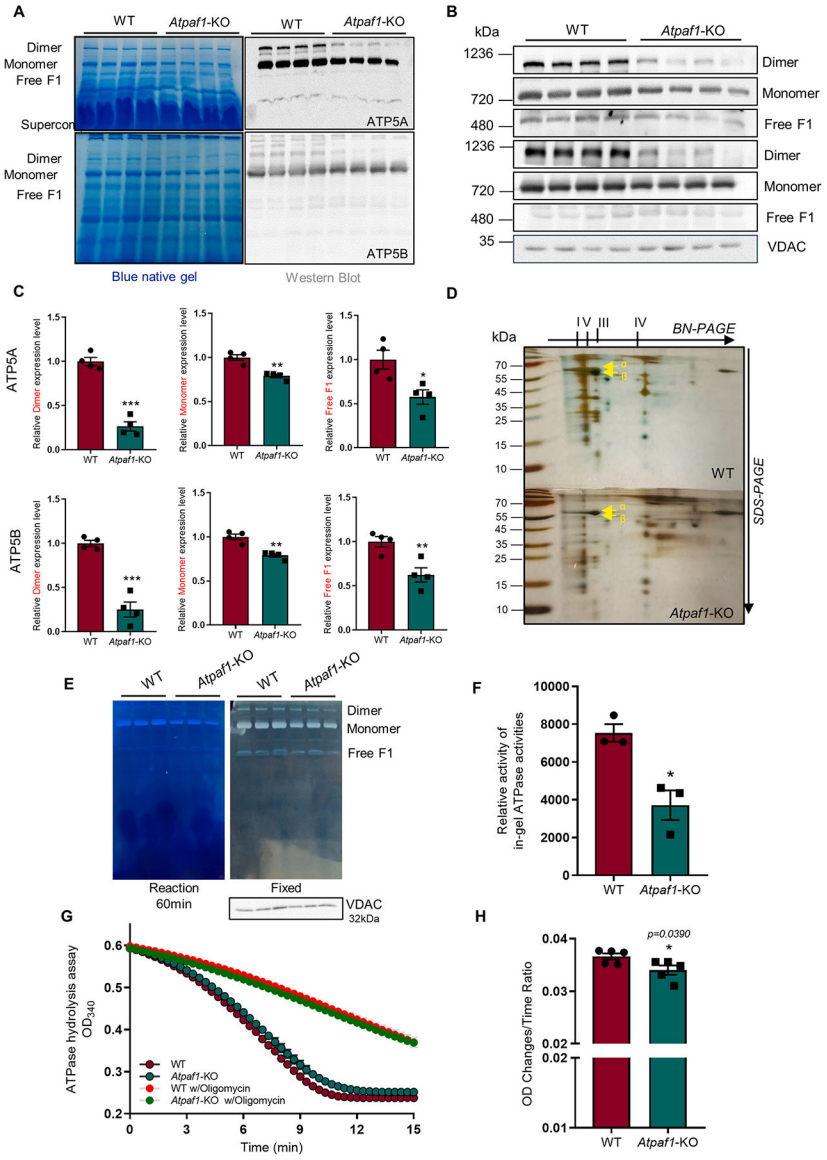

Fig. 3.

Absence of ATPAF1 reduces dimerization and overall content of F1Fo-ATP Synthase, impairing ATP synthase activity. (A) Separation of heart mitochondrial protein solubilized by digitonin using a detergent/protein ratio of 6 (g/g) and immunoblotted with anti-α and β subunit of ATP synthase antibody (n = 4). (B) Images of Western blots bands for dimer, monomer, free F1 and VDAC. (C) Quantitative data showing the relative expression of dimer, monomer and free F1 between WT and *Atpaf1*-KO mice. VDAC was used as protein loading control (n = 4). (D) Analysis of subunits of the mitochondrial ATP synthase complex from mice heart tissue by 2D BN-PAGE. Cardiac mitochondrial protein complexes were first separated by BN-PAGE. Afterwards, the lane for each of WT and *Atpaf1*-KO mice were processed by 2D BN-PAGE, then the gels were conducted with silver staining. Arrows mark α- and β-subunit separated from WT and *Atpaf1*-KO mitochondria protein. (E) Representative images of In-gel ATPase activity (n = 3). (F) Quantitative data

of In-gel ATPase activity and VDAC was used as protein loading control. The samples were cardiac mitochondria isolated from 16 to 18 weeks WT and *Atpaf1*-KO mice. (G) ATPase hydrolysis assay for cardiac mitochondria. (n = 5). (H) Quantitative analysis of the activity levels from (G). The experiment shown above is representative of three independent experiments. *p < 0.05, **p < 0.01, ***p < 0.001 vs wild type. Values are expressed as mean ± SEM.

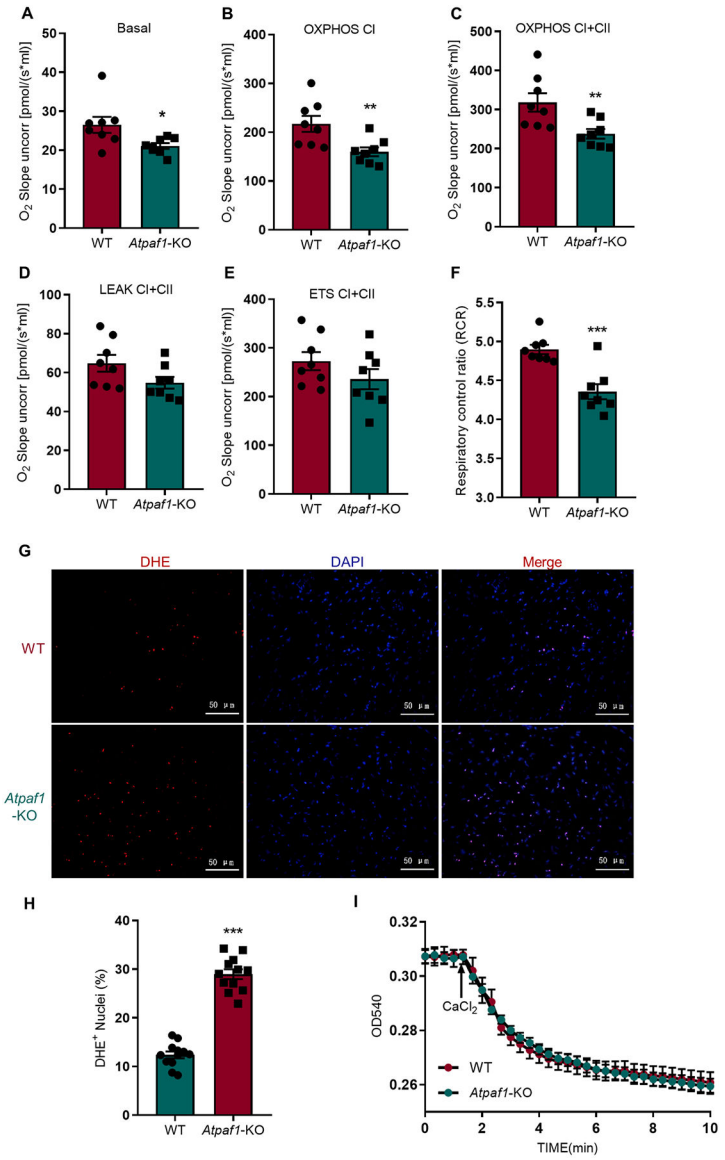

Fig. 4.

Deficiency of ATPAF1 weakens cardiac mitochondrial respiration capacities and increases myocardial ROS levels in *Atpaf1*-KO mice. (A-F) Real-time oxygen consumption experiments in WT and *Atpaf1*-KO groups. Fresh mitochondrial proteins were extracted from 18 to 20 weeks WT and *Atpaf1*-KO mice. Quantitative analysis of different stages of the mitochondrial respiratory process (n = 8). (A) Basal mitochondrial respiration capacities (Routine). (B) Phosphorylating respiration capacities via convergent input through complex I ($OXPHOS_{CI}$). (C) Maximal phosphorylating respiration capacities via convergent input through complexes I and II ($OXPHOS_{CI+CII}$). (D) The maximal uncoupled respiratory capacities of ETS (ETS_{CI+CII}). (E) Inhibition of the phosphorylation system by oligomycin ($LEAK_{CI+CII}$). (F) Respiratory control ratio (RCR). (G) Representative images of frozen heart sections stained with DHE (red) and DAPI (blue) (n = 3). (H) Quantitative analysis of the DHE-positive nucleus (12 fields from 3 mice per group). (I) Calcium-induced swelling

rates of mitochondria isolated from mice heart (n = 5). *p < 0.05, **p < 0.01, ***p < 0.001 vs wild type. Values are expressed as mean ± SEM.

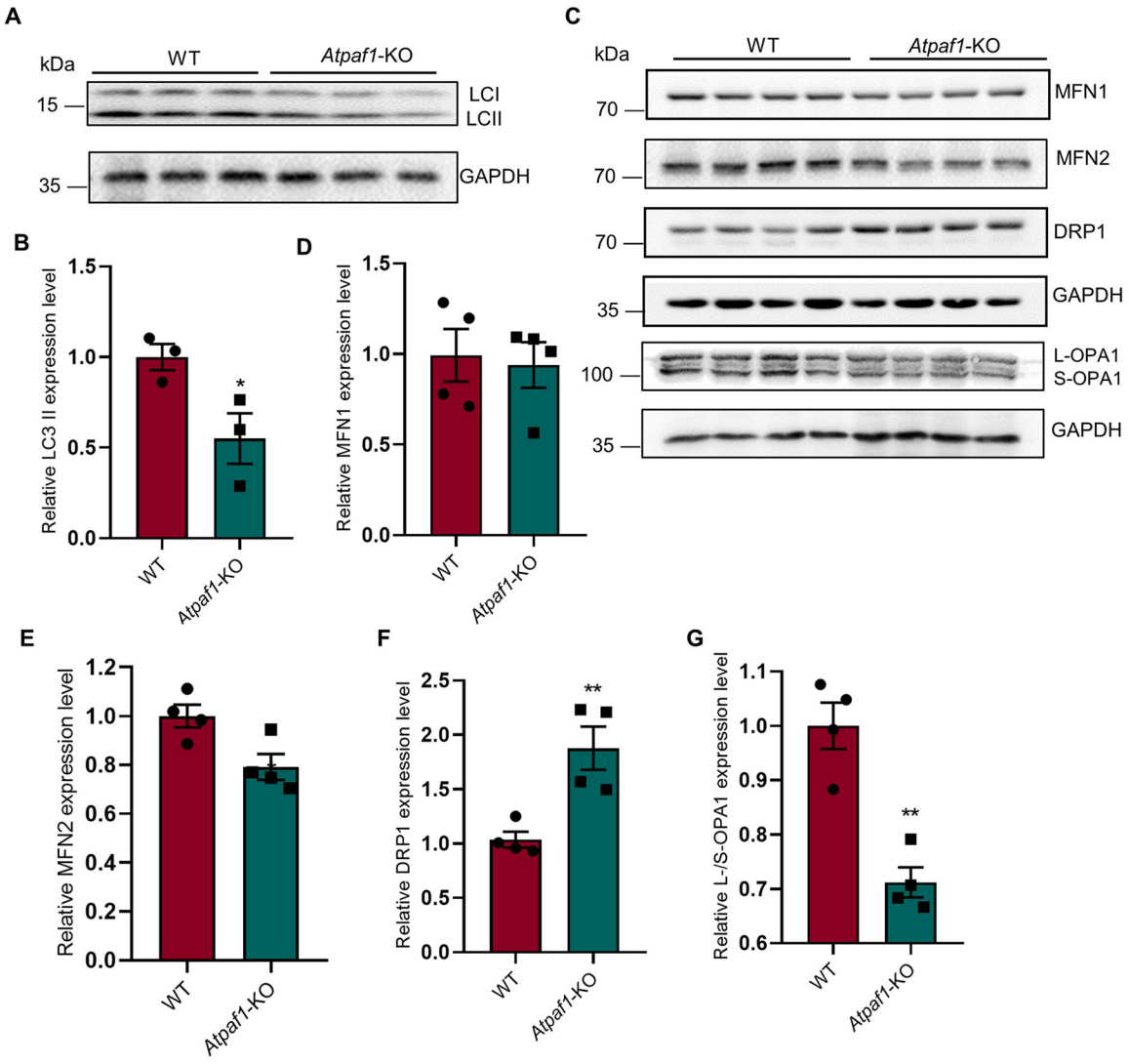

Fig. 5.

The expression of autophagy-related protein and mitochondrial dynamics-related proteins. (A) Total protein expression of LC3 protein *in vivo* were determined by Western blots. GAPDH was used as protein loading control. (B) Quantitative analysis of the blots. (C) The expression of mitochondrial dynamics-related proteins. (D-G) Quantitative analysis of the blots. The experiment shown above is representative of three independent experiments. *$p < 0.05$, **$p < 0.01$ vs wild type. Values are expressed as mean ± SEM.

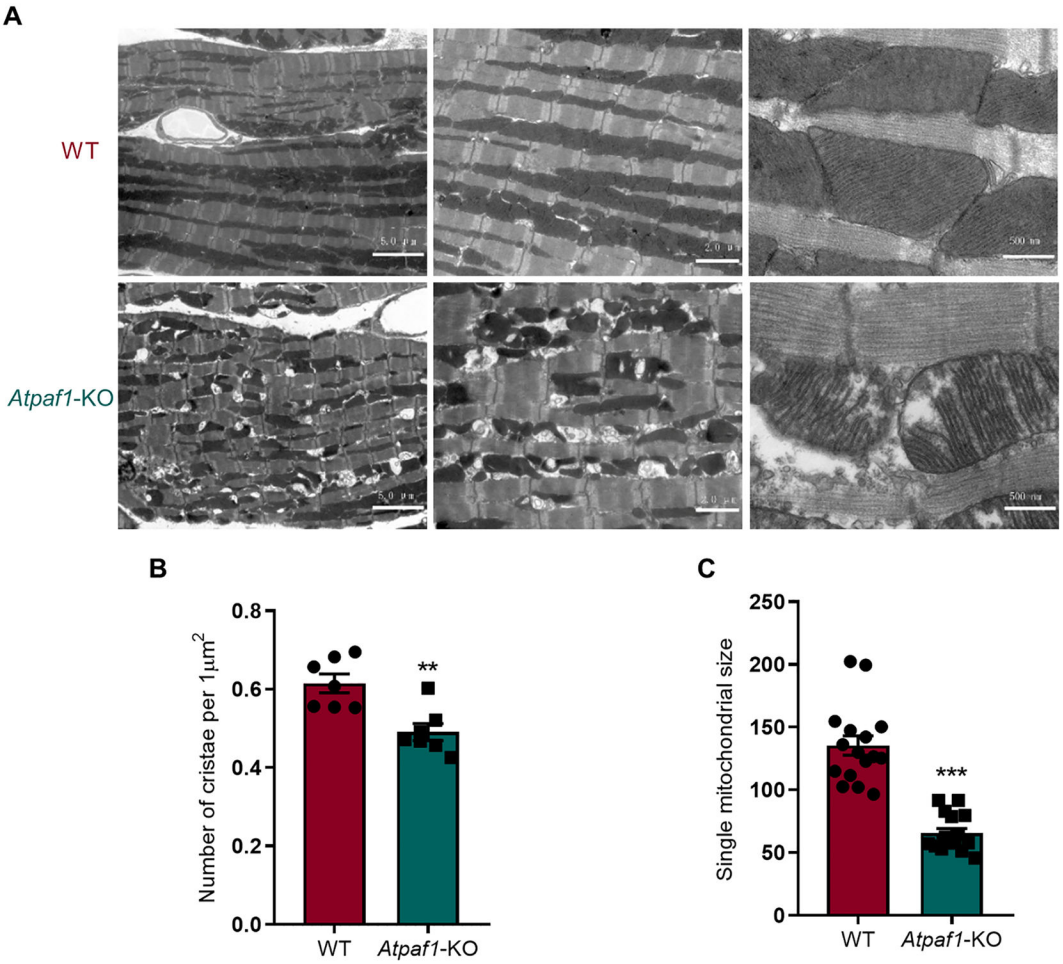

Fig. 6.

Cardiac mitochondrial ultrastructure of *Atpaf1*-KO mice. (A) Representative TEM micrographs of 15–18 weeks old WT and *Atpaf1*-KO mouse hearts (n = 4). (B-C) Quantitative analyses of mitochondrial abundance and morphometry. **p < 0.01, ***p < 0.001 vs wild type. Values are expressed as mean ± SEM.

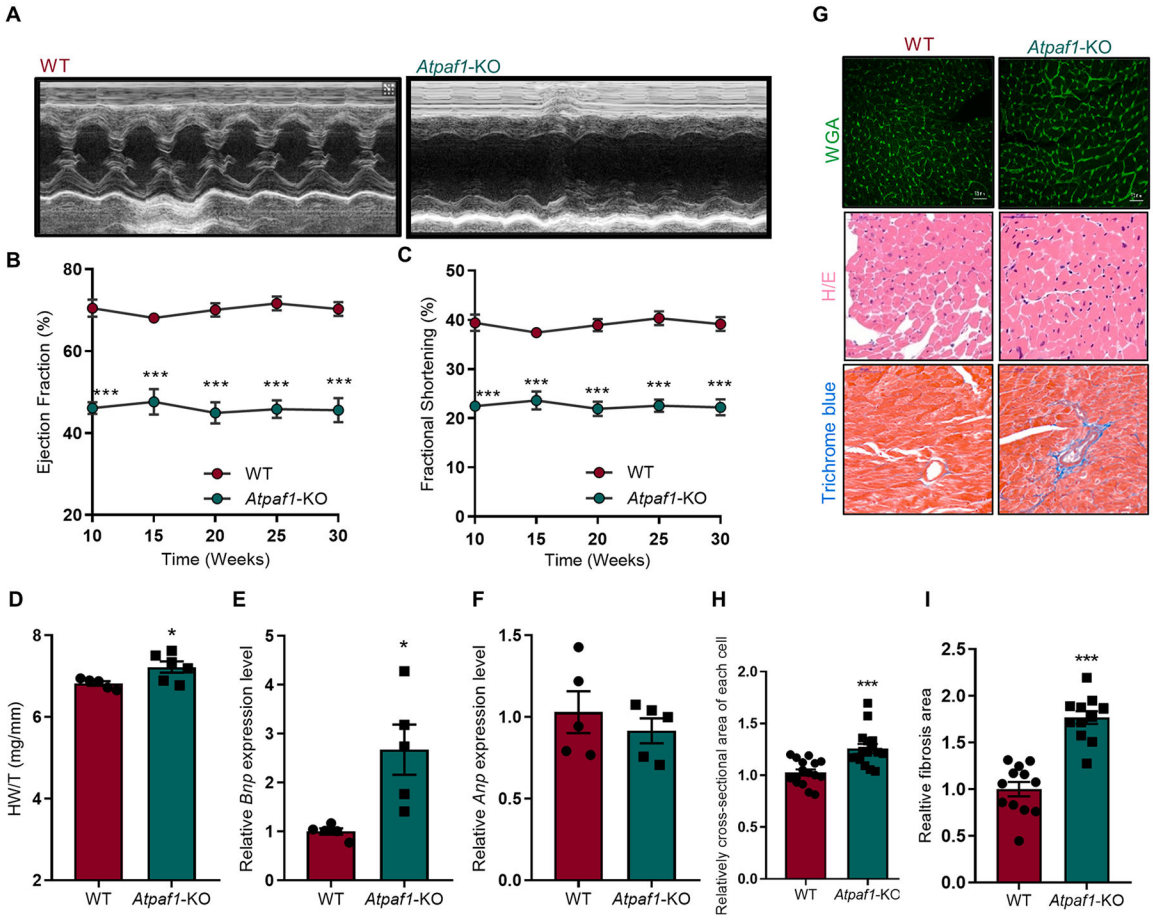

Fig. 7.

ATPAF1 deficiency in mice leads to cardiac dysfunction and LV remodeling. (A-C) Echocardiography of left ventricular structure and function of WT and *Atpaf1*-KO mice (n = 4–7). (A) Representative images of echocardiograms. (B) Echocardiographic measurement of LV ejection fraction (EF%). (C) Echocardiographic measurement of fractional shortening (FS%). (D) Heart weight to tibia length (HW/T, mg/mm) (n = 5–6). (E-F) Relative mRNA expression levels of *Anp* and *Bnp* were determined by qPCR. The housekeeping gene *Actin* was used for normalization (n = 3). (G) Representative histological images with WGA, HE and Masson's trichrome staining of heart sections taken from 18 to 22 week mice (n = 4). (H) Quantitative data of the cross-sectional area of each cell. (I) Quantification of fibrotic area from Masson's trichrome staining photographs. The experiment shown above is representative of three independent experiments. *p < 0.05, ***p < 0.001 vs wild type. Values are expressed as mean ± SEM.

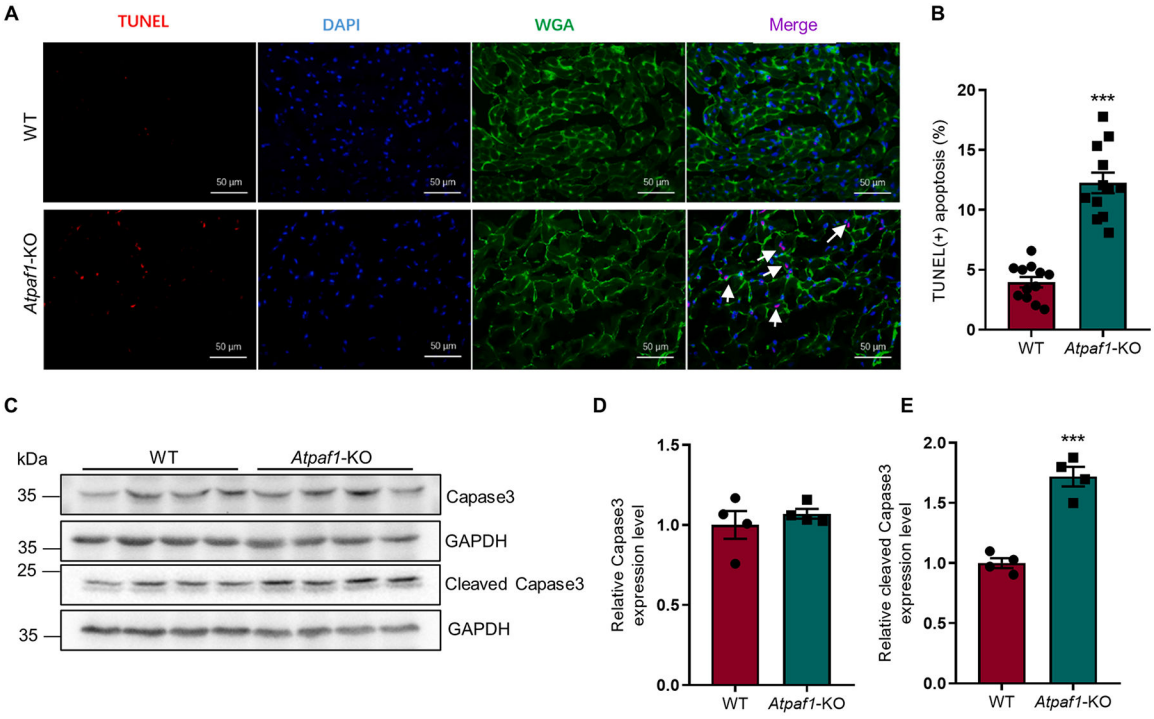

Fig. 8.

Cardiomyocyte apoptosis in *Atpaf1*-KO mice. (A) Representative photomicrographs for TUNEL staining (red) of heart sections from WT and *Atpaf1*-KO mice (n = 3). (B) Quantitative data of TUNEL-positive cells. (C) Western blots of Caspase3 and cleaved Caspase3. GAPDH was used as loading control (n = 4). (D-E) Quantitative protein expression of Caspase3 and cleaved Caspase3. ***p < 0.001 vs wild type. Values are expressed as mean — SEM.